Draft version January 22, 2025
Typeset using LaTeX **twocolumn** style in AASTeX631

# Emergence of two inertial sub-ranges in solar wind turbulence: dependence on heliospheric distance and solar activity

Shiladittya Mondal [1], Supratik Banerjee [1], and Luca Sorriso-Valvo [2,3]

[1] Department of Physics, Indian Institute of Technology Kanpur, Kanpur 208016, India
[2] Institute for Plasma Science and Technology (ISTP), CNR, Bari, Italy
[3] Space and Plasma Physics, School of Electrical Engineering and Computer Science, KTH Royal Institute of Technology, Stockholm, Sweden

## ABSTRACT

The solar wind is highly turbulent, and intermittency effects are observed for fluctuations within the inertial range. By analyzing magnetic field spectra and fourth-order moments, we perform a comparative study of intermittency in different types of solar wind measured during periods of solar minima and a maximum. Using eight fast solar wind intervals measured during solar minima between 0.3 au and 3.16 au, we found a clear signature of two inertial sub-ranges with $f^{-3/2}$ and $f^{-5/3}$ power laws in the magnetic power spectra. The intermittency, measured through the scaling law of the kurtosis of magnetic field fluctuations, further confirms the existence of two different power laws separated by a clear break. A systematic study on the evolution of the said sub-ranges as a function of heliospheric distance shows correlation of the break scale with both the turbulence outer scale and the typical ion scales. During solar maximum, we analyzed five intervals for each of Alfvénic fast, Alfvénic slow and non-Alfvénic slow solar wind. Unlike the case during the solar minima, the two sub-ranges are no longer prominent and the Alfvénic slow wind is found to be in an intermediate state of turbulence compared to that of the fast wind and the usual non-Alfvénic slow wind.

*Keywords:* Solar wind (1534) — Space plasmas (1544) — Interplanetary turbulence (830) — Magnetohydrodynamics (1964)

## 1. INTRODUCTION

The solar wind is the most accessible natural laboratory for studying turbulence in space plasmas (Bruno & Carbone 2013). The dynamic solar activity and the diversity of the originating regions produce solar wind with a variety of characteristics, the most evident being the plasma speed. While the fast solar wind (FSW, $> 550\ km\ s^{-1}$) mainly emanates from the polar coronal holes, the slow solar wind (SSW, $< 400\ km\ s^{-1}$) is believed to be originated from equatorial streamers (Belcher & Davis Jr. 1971; Smith et al. 1978; Phillips et al. 1995). During high solar activity, however, both FSW and SSW are distributed at all latitudes instead of being confined exclusively to polar and equatorial regions, respectively. Another interesting feature of FSW is the high Alfvénicity *i.e.* high correlation (or anti-correlation) between velocity fluctuations ($\mathbf{v}$) and $\mathbf{b}$ ($= \mathbf{B}/\sqrt{\mu_0 \rho}$, where $\mathbf{B}$ the magnetic field fluctuation and $\rho$ the mass density) in contrast with the SSW comprising of weak $\mathbf{v}$-$\mathbf{b}$ correlations. This one-to-one correspondence, however, does not strictly hold during high solar activity, as a third type of wind is also observed. This wind, termed as Alfvénic slow solar wind (ASSW), has speed similar to that of the slow wind but is surprisingly permeated with high Alfvénicity (Marsch et al. 1981; D'Amicis et al. 2011; D'Amicis & Bruno 2015). The degree of Alfvénicity correlates with the nature of turbulence in different types of solar winds. A high degree of Alfvénicity corresponds to an imbalance between the Elsässer variables, $\mathbf{z}^{\pm} = \mathbf{v} \pm \mathbf{b}$, thus leading to less developed turbulence whereas low Alfvénicity corresponds to comparatively more developed turbulence owing to the balance between them. At scales greater than the ion-inertial length ($d_i$), a longer $k^{-5/3}$ energy power spectrum is therefore observed for the slow wind whereas a comparatively shorter $k^{-5/3}$ spectrum is observed in the Alfvénic fast wind (Bruno & Carbone 2005; Bruno & Carbone 2013; D'Amicis et al. 2018).

These observed spectra are universal in solar wind turbulence and are consistent with self-similar energy cascade (Kolmogorov phenomenology) within the inertial range. In physical space, universal energy cascade is obtained in terms of the linear scaling law for the third-order moments of velocity and magnetic field fluctuations (Sorriso-Valvo et al. 2007; Banerjee et al. 2016; Marino & Sorriso-Valvo 2023). In order to assure a self-similar cascade, the kurtosis $K$ (the normalised fourth-order moment of the fluctuations) should be scale invariant. For a turbulent flow, one such possibility is the case of quasi-Gaussian PDFs where the third-order moment (skewness) is non-zero but the K is roughly equal to that of a Gaussian distribution.

However, careful studies in turbulent fluids and plasmas consistently show a departure from self-similarity as one moves towards the smaller length scales within the inertial range. This departure, known as inertial-range intermittency, is characterised by the large tails of the PDFs at those scales. In particular, intermittency effects are quantified by the deviation from the self-similar scaling laws of the higher-order moments (Frisch 1995; Biskamp 2003; Banerjee 2014). Instead of using arbitrary higher-order moments, the kurtosis is often used as a practical measure of intermittency and a higher probability of extreme events leads to its increase with decreasing length scale $\ell$. From a physical point of view, this implies that the small-scale coherent structures, such as the vortices, current sheets, etc., generated due to nonlinear interactions, do not fill the available space in a self-similar way nor are randomly distributed, but rather tend to form inhomogeneously distributed clusters of bursts (Frisch 1995; Sorriso-Valvo et al. 1999; Bruno et al. 2003).

While the solar wind expands and accelerates through the heliosphere, the turbulence becomes more developed, with the fluctuations being majorly energized by the nonlinear interactions between the oppositely propagating Alfvén waves (Chandran 2018), switchbacks (Bale et al. 2021; Sakshee et al. 2022), large-scale structures, and instabilities (Bavassano et al. 1982a; Roberts et al. 1992). Using *in-situ* spacecraft data, a steepening of the magnetic power spectra was found with increasing heliospheric distance ($R$) in the inner-heliosphere whereas, a similar steepening for the velocity power spectra was also observed beyond 1 au (Bavassano et al. 1982b; Roberts 2010). In addition, a decrease in **v-b** correlations and a broadening of the inertial range was also found as $R$ increases (Bavassano et al. 1998; Bavassano et al. 1982b; Davis et al. 2023). Recently, using high resolution data of the Parker Solar Probe it has been suggested that the magnetic spectral index evolves from $-3/2$ near the Sun (as close as 0.17 au) to a more developed $-5/3$ at 1 au (Alberti et al. 2020; Chen et al. 2020; Shi, C. et al. 2021; Sioulas et al. 2023a). These observations are consistent with the idea of radial evolution of solar wind turbulence into more developed states and the non-adiabatic heating of the medium with increasing heliospheric distance (Marsch et al. 1982; Cranmer et al. 2009; Hellinger et al. 2011). In addition, a power law behaviour for the kurtosis (Bruno et al. 2003; Di Mare et al. 2019; Carbone et al. 2021; Hernández et al. 2021) and an increase in intermittency in solar wind turbulence have been observed at greater heliospheric distances (Sioulas et al. 2022; Sorriso-Valvo et al. 2023). Using the magnetic data of Helios 2, Sorriso-Valvo et al. (2023) observed a break in the scaling of $K$ of the magnetic field fluctuations in FSW, during solar minimum. They provided a plausible explanation suggesting this observed break to be associated with the $f^{-1}$ break in the magnetic power spectrum of FSW. However, clear disparity is observed between the scales corresponding to the breaks in kurtosis scaling and the power spectra. A break in both the spectral density and the higher-order structure functions has also been observed (Wicks et al. 2011; Wu et al. 2022; Telloni 2022; Sioulas et al. 2023b; Wu et al. 2023). However, the nature of such break and its implications on the dynamics of the solar wind turbulence have not been investigated in detail yet.

In this paper, we revisit the aforementioned problem and carry out a systematic study to provide an explanation for the break observed in the kurtosis scaling. Using the *in-situ* data of Helios and Ulysses during solar minima, we show the kurtosis break is primarily associated with an observed break between two inertial sub-regimes of magnetic power spectra, having $-3/2$ and $-5/3$ spectral indices, respectively. In addition, we also study the radial evolution of the break scale to characterise the solar wind turbulence as a function of the heliospheric distance. During a solar maximum, a comparative study of FSW, ASSW and SSW shows a clear distinction of these three types of wind according to the degree of turbulence and the degree of intermittency, along with some insights on the origin of ASSW. In Sections 2 and 3, we briefly describe the data and methodologies used for the analysis. Section 4 provides the results obtained in our study during solar minima (4.1) and maxima (4.2), respectively. Finally, in Section 5, we summarize our findings and conclude.

## 2. DATA SELECTION

For our analysis, we have used *in-situ* data from the Helios and Ulysses spacecraft data repository publicly available at NASA CDAWeb (https://cdaweb.gsfc.nasa.gov) and AMDA science analysis system (https://amda.irap.omp.eu). The plasma data for Helios and Ulysses have been obtained from the E1 Plasma Experiment instrument and the

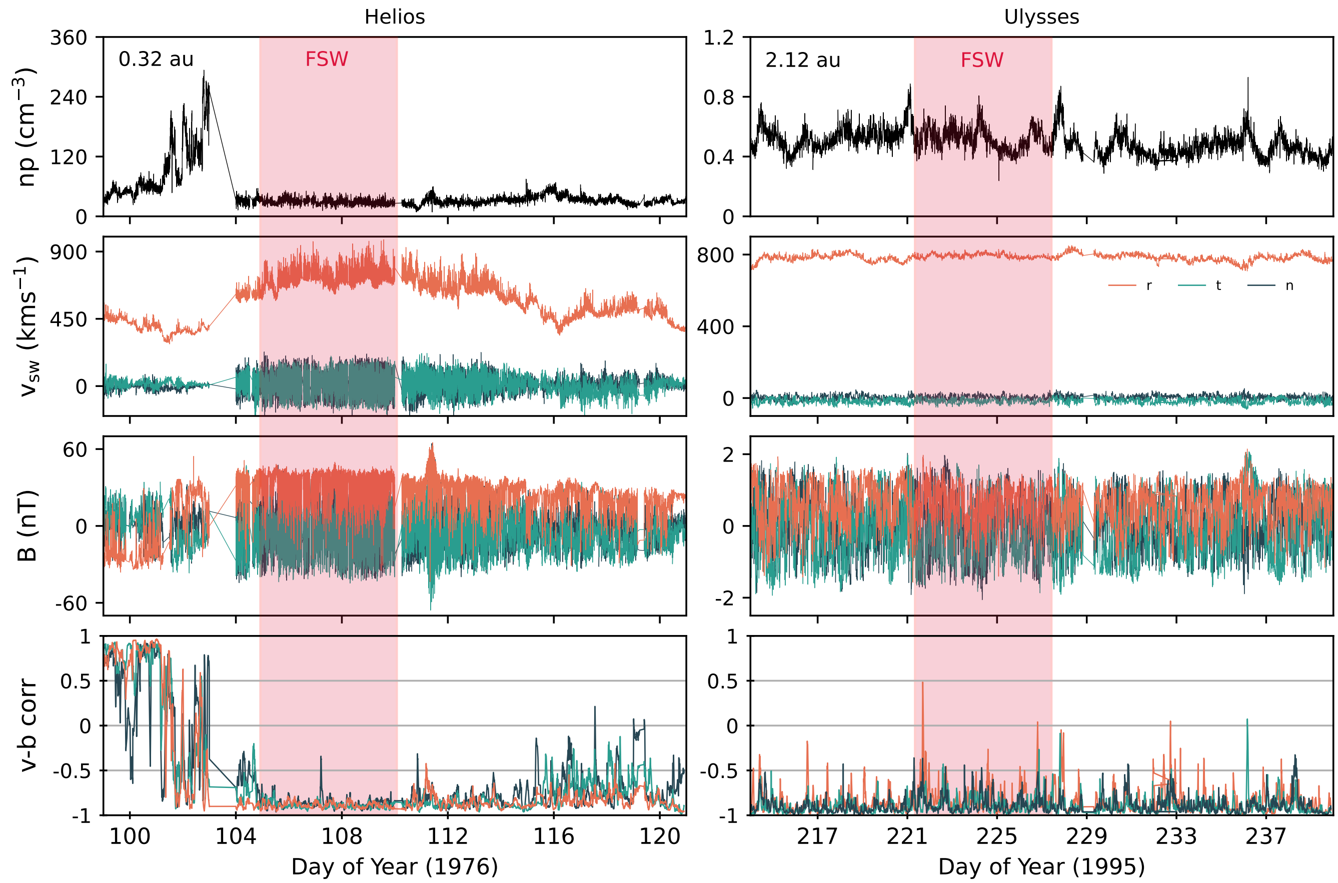


**Figure 1.** FSW intervals indicated by red boxes using Helios (left) and Ulysses (right) data, during solar minima. Top to bottom: proton number density, solar wind speed, interplanetary magnetic field, correlation co-efficient between the components of proton velocity and magnetic field computed over a 2 hr window.

Solar Wind Observations Over the Poles of the Sun (SWOOPS) instrument, respectively. For magnetic power spectrum and kurtosis scaling, we use 6 s resolution magnetic-field data from the E3 Flux-gate Magnetometer (FGM) onboard Helios and 1 s resolution magnetic field data from the Vector Helium Magnetometer (VHM) onboard Ulysses spacecraft. During a declining phase of solar activity near a solar minimum between 1975 and 1976, Helios 1 and 2 recorded several streams of FSW from a coronal hole (or the same source), which sustained through nearly two solar rotations (Bruno et al. 2003). Several intervals of the fast wind expelled from this coronal hole were also identified by Perrone et al. (2018). In particular, for our current analysis, we use the streams - A3, A6, A7, and A8, ranging from 0.3 au to 1 au, mentioned therein. Each chosen interval (i) contains negligibly small amount of data gaps, (ii) is free of any considerable mean trend, and (iii) turns up to be reasonably stationary. The stationarity is assured by the approximate constant average of sub-intervals of different lengths. Extending our analysis beyond 1 au, we use four intervals of FSW at varying heliospheric distances (F1 - F4 as listed in Table - 1), recorded by Ulysses during the years 1995-1996. Typical features of certain FSW intervals in the inner and outer heliosphere used in our analysis with high v-b correlations are shown in Fig. 1.

In order to interpret our findings, we also need to compute the co-spectra of cross-helicty $\sigma_c$ (see Section 3), for which we have used the 40.5 s resolution magnetic field and proton velocity data from the E3 FGM and the E1 Plasma Experiment instrument onboard Helios. We use degraded resolution for the magnetic field data in order to keep coherence with the available plasma data from the data repository. A similar analysis cannot be done using the plasma data of Ulysses where the data resolution is 240 s, and hence cannot be used to capture the required length scales of our interest.

During solar maximum, five Ulysses intervals each for the three types of solar wind were selected following similar methods prescribed in D'Amicis et al. (2018) based on their speed, proton density, and Alfvénic correlations (see Table 1). A particular case study represents several properties of the different types of wind within a 20-day

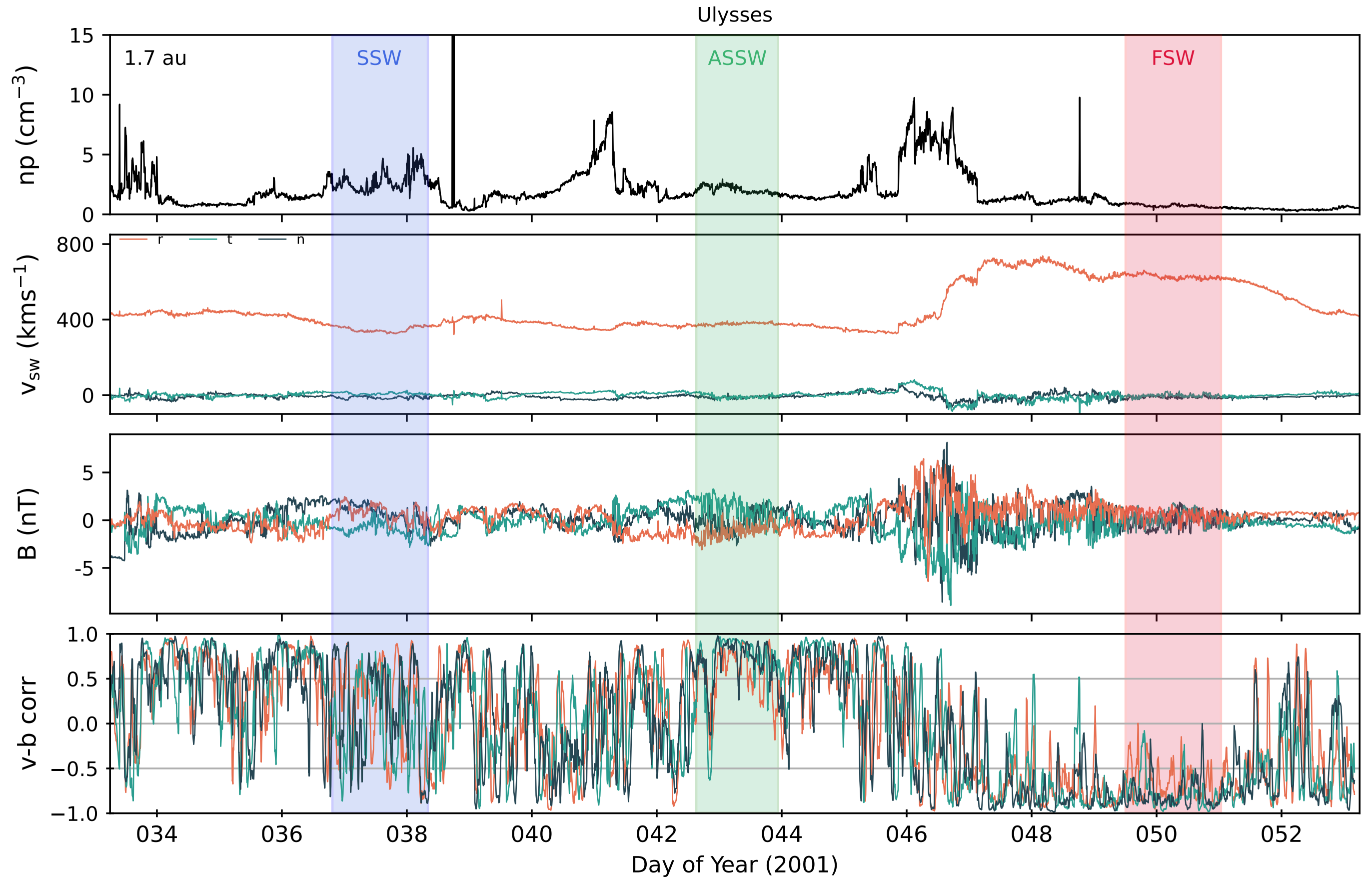


**Figure 2.** Different Ulysses intervals of SW during a period of solar maximum. Top to bottom: proton number density, solar wind speed, interplanetary magnetic field, correlation co-efficient between the components of proton velocity and magnetic field computed over a 2 hr window. Blue, green and red boxes represent SSW, ASSW, and FSW intervals, respectively.

interval (see Fig. 2). While ASSW looks very similar to SSW with respect to the flow speed ($< 400$ km/sec), it is characterised by low proton density ($\sim 1$ particle/cm$^3$) and high Alfvénicity ($\sim 0.6$) similar to FSW. These findings are in agreement with previous studies (Belcher & Davis Jr. 1971; Marsch et al. 1981; D'Amicis & Bruno 2015).

## 3. ANALYSIS METHOD

Our analysis is mainly based on the computation of (i) the kurtosis ($K$) or the normalized fourth-order moments of magnetic field fluctuations, (ii) the magnetic power spectral density ($PSD$), and (iii) the cross-helicity co-spectra ($\hat{\sigma_c}$). All the data sets were made evenly sampled by interpolating the data gaps before using for any of the computations.

Since all the intervals used in our study are permeated by super-Alfvénic solar wind, one can practically use Taylor's hypothesis, which means if the phase speed of the fluctuations is much smaller than the flow speed of the solar wind, the fluctuations can be considered as frozen (or slowly evolving) as the flow sweeps the probe (Taylor 1938). When using single-point measurements in the form of a time series, the only accessible direction for the increments is along the bulk flow. This provides an equivalence between the longitudinal (along the flow) length scale $\ell$ and the corresponding time scale $\tau$ as $\ell = V_{sw}\tau$, where $V_{sw}$ is the mean solar wind speed. Therefore, we define the increments of the $i^{th}$ component (with $i = r, t, n$) of the magnetic field as $\Delta B_i(t,\tau) = B_i(t+\tau) - B_i(t)$. In order to capture both magnitudinal and directional fluctuations of **B**, we define the $n^{th}$ order structure function as:

$$S_n(\tau) = \left\langle \left[ \sum_i (\Delta B_i)^2 \right]^{n/2} \right\rangle, \tag{1}$$

where $\langle \cdot \rangle$ represents the ensemble average (Bruno et al. 2003). The corresponding kurtosis (K) is then calculated using the standard expression:

$$K(\tau) = \frac{S_4(\tau)}{[S_2(\tau)]^2}. \tag{2}$$

Note that, when each $\Delta B_i$ follows a Gaussian distribution with zero mean, $K(\tau)$ is equal to 5/3 (see appendix

**Table 1.** Intervals of FSW, ASSW and SSW used in our study. The intervals A3, A7, A8 (Helios-2) and A6 (Helios-1) are mentioned in Perrone et al. (2018) as well. The other intervals with abbreviations F# (fast), S# (slow), AS# (Alfvénic-slow) are from Ulysses spacecraft.

| Label | Year | Time Interval (MM-DD-HH) | $v_{sw}$ (km/sec) | R (au) |
|---|---|---|---|---|
| | | Solar minimum | | |
| A8 | 1976 | 04-14-14 – 04-22-01 | 728.9 | 0.30 |
| A6 | 1976 | 03-14-10 – 03-19-13 | 624.3 | 0.41 |
| A7 | 1976 | 03-15-18 – 03-18-03 | 620.9 | 0.65 |
| A3 | 1976 | 01-21-21 – 01-25-10 | 633.1 | 0.98 |
| F1 | 1995 | 01-21-00 – 01-27-16 | 745.7 | 1.44 |
| F2 | 1995 | 08-09-19 – 08-15-12 | 795.0 | 2.10 |
| F3 | 1995 | 11-12-00 – 11-18-00 | 795.6 | 2.75 |
| F4 | 1996 | 01-16-00 – 01-22-00 | 765.7 | 3.16 |
| | | Solar maximum | | |
| F5 | 2001 | 08-16-02 – 08-18-02 | 734.4 | 1.64 |
| F6 | 2001 | 09-09-14 – 09-11-14 | 753.9 | 1.80 |
| F7 | 2001 | 08-26-10 – 08-28-10 | 690.9 | 1.71 |
| F8 | 2001 | 02-18-07 – 02-20-07 | 626.6 | 1.69 |
| F9 | 2001 | 03-13-00 – 03-15-00 | 694.9 | 1.56 |
| S1 | 2001 | 02-08-20 – 02-10-20 | 353.5 | 1.53 |
| S2 | 2001 | 05-01-15 – 05-03-15 | 385.9 | 1.35 |
| S3 | 2001 | 06-21-23 – 06-23-23 | 387.3 | 1.41 |
| S4 | 2001 | 07-05-08 – 07-07-08 | 413.7 | 1.34 |
| S5 | 2001 | 06-05-12 – 06-07-12 | 400.0 | 1.47 |
| AS1 | 2001 | 07-27-14 – 07-29-14 | 367.4 | 1.76 |
| AS2 | 2001 | 05-06-05 – 05-08-05 | 347.9 | 1.36 |
| AS3 | 2001 | 06-29-04 – 07-01-04 | 430.4 | 1.38 |
| AS4 | 2001 | 05-16-06 – 05-18-06 | 300.7 | 1.43 |
| AS5 | 2001 | 03-29-12 – 03-31-12 | 469.0 | 1.35 |

Section A). For a self-similar, non intermittent flow, in the inertial range of scales (namely much smaller than the energy-injection scales and larger than the dissipative scales) the $n^{th}$ order structure function is expected to scale as $S_n(\tau) \propto \tau^{np}$, where $p$ is a phenomenological constant (Frisch 1995). It is therefore straightforward to see that $K$ becomes independent of $\tau$. However, in the presence of intermittency, this linear scaling does not hold any longer and the simplest intermittency model can be given as $S_n(\tau) \propto \tau^{np+q(n)}$, where $q(n)$ is a non-linear correction accounting for the intermittent structures. For the kurtosis, this leads to a power-law scaling $K(\tau) \sim \tau^{-\kappa}$, with $\kappa = q(4)/2q(2)$. Such a scaling, universally observed in fluid turbulence, has recently been described in the case of solar wind turbulence as well (Di Mare et al. 2019; Hernández et al. 2021; Sorriso-Valvo et al. 2023). In this work, we study the scaling properties of $K$ of the magnetic field fluctuations at different heliospheric distances.

Finally, the magnetic energy spectra and normalized cross-helicity co-spectra are defined as $PSD = \hat{B_i}^{\dagger}\hat{B_i}$ and $\hat{\sigma_c} = (\hat{b_i}^{\dagger}\hat{v_i} + \hat{v_i}^{\dagger}\hat{b_i})/(|\hat{b_i}|^2 + |\hat{v_i}|^2)$ respectively, where $\hat{B_i}$, $\hat{b_i}$ and $\hat{v_i}$ are the Fourier transforms (FT) of $B_i$, $b_i$ and $v_i$, respectively, with summation being intended over the repeated indices (where $i = r, t, n$).

## 4. RESULTS AND DISCUSSIONS

### 4.1. *Observations during Solar Minimum*

During a period of solar minimum in 1976, using data from Helios spacecraft, we study FSW streams in the inner heliosphere (at $0.3, 0.41, 0.65$, and $0.98$ au) from a sustained coronal hole near the ecliptic plane. Beyond 1 au, FSW streams are studied using Ulysses data collected during the 1995-1996 solar minimum, at varying heliospheric distances (at $1.44, 2.1, 2.75$, and $3.16$ au), which were also measured at different latitudes. In Fig. 3, we have drawn the magnetic power spectral traces, smoothed using a running mean window. Top panels refer to Helios intervals, while bottom panels to Ulysses. As typically observed in the Alfvénic solar wind, at low frequencies we can identify a large-scale, energy-containing range (white background in the figure), where the power decays as $\sim f^{-1}$. Fitted power laws and the corresponding scaling exponents are shown as green lines. A break identifies a clear change in the power-law scaling exponent, as indicated by vertical dashed lines. Such break can be associated with the correlation scale of the turbulence. The low-frequency range is clearly visible in Helios data, while it is only indicatively present in the Ulysses intervals. This is consistent with the well-known shift of the correlation scale towards lower frequency with increasing $R$ in the solar wind (Davis et al. 2023). The $f^{-1}$ range is followed by the usual inertial range of turbulence, where the spectrum roughly follows an $f^{-5/3}$ power law dependence (Bruno & Carbone 2005; Bruno & Carbone 2013). However, a more accurate inspection shows that a further break emerges within such range, indicated by the vertical dot-dashed lines separating the light and deeper blue shaded areas in Fig. 3. Although the dynamical range of frequencies is relatively short, for intervals other than that at 3.16 au, it is possible to identify two different sub-ranges with different power laws

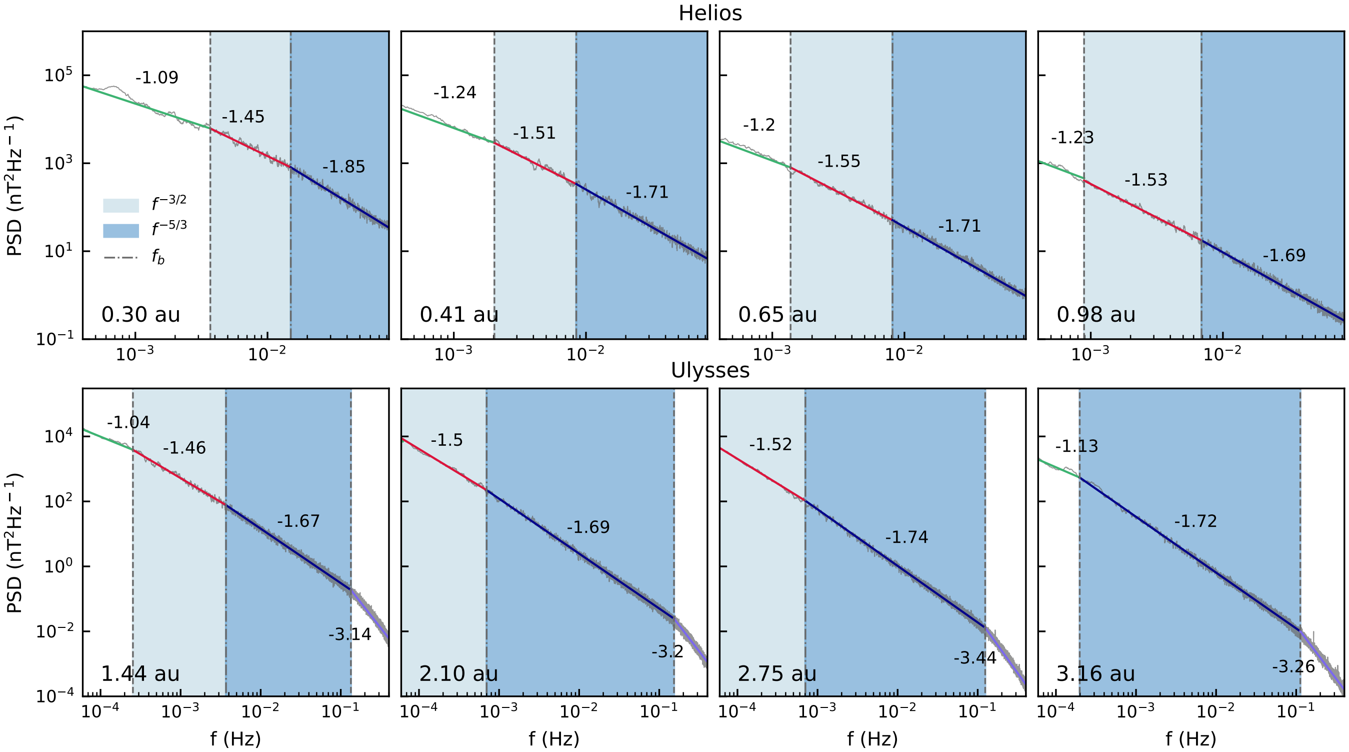


**Figure 3.** Magnetic power spectral trace of FSW intervals (smoothed using a running mean window) at varying heliospheric distances $R$ during solar minima. Top row: Helios data, bottom row: Ulysses data. In all panels, the distance of the interval from the sun is indicated. Vertical lines indicate the $f^{-1}$ break (dashed), the newly observed break $f_b$ (dot-dashed, separating the light and deep blue areas jointly forming the traditional inertial range), and the ion-scale break (Ulysses only). In each range, a power-law fit is shown (colored lines) along with the corresponding spectral exponent.

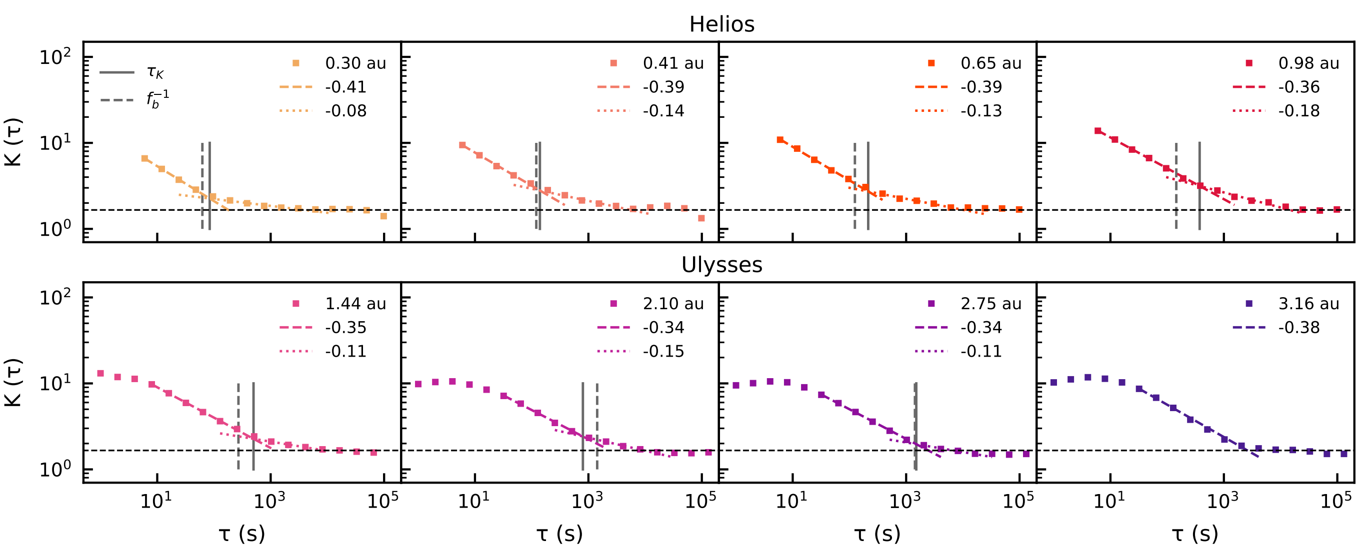


**Figure 4.** Kurtosis $K(\tau)$ of magnetic field fluctuations for several intervals of FSW during periods of solar minima. Top panels: Helios data (year 1976) in the inner heliosphere from a sustained coronal hole. Bottom panels: Ulysses data (years 1995-1996) in the outer heliosphere at varying distances and latitudes (the distance of each interval is indicated and associated to a given color). Power-law fits and the corresponding scaling exponents are indicated. Vertical lines indicate the observed break, $\tau_K$ (solid lines), and the timescale corresponding to the spectral break, $1/f_b$ (dashed).

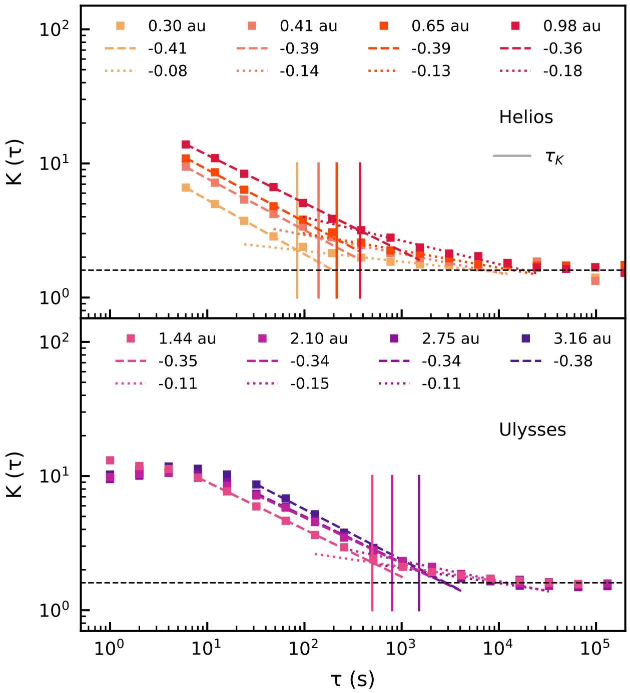


**Figure 5.** Consolidated plot of the kurtosis $K(\tau)$ scalings of the FSW intervals during solar minima. Top panel: Helios data ($R < 1$ au); Bottom: Ulysses data ($R > 1$ au). Vertical full lines indicate the break, $\tau_K$, shifting towards larger scales with $R$.

as demonstrated by the red and blue lines, with the associated scaling exponents indicated nearby. In the lower-frequency range (light blue background), the spectral index approaches -3/2, whereas at larger frequencies (deep blue background), the spectra show a transition to a -5/3 spectral index usually observed in non-Alfvénic solar wind (Bruno & Carbone 2005; Bruno & Carbone 2013; Alexandrova et al. 2009; D'Amicis et al. 2018). In isotropic turbulence, whereas an $f^{-5/3}$ scaling often represents an energy cascade by eddy fragmentation in strong turbulence, $f^{-3/2}$ scaling can possibly be explained by an energy cascade through the sporadic interaction of Alfvénic wave packets in MHD turbulence (Kolmogorov 1941; Iroshnikov 1963; Kraichnan 1965). However, $-5/3$ and $-3/2$ power laws can also be obtained under various circumstances if anisotropy is taken into account (Goldreich & Sridhar 1995; Goldreich & Sridhar 1997; Boldyrev 2006; Chandran et al. 2015). Irrespective of the true nature of energy cascade, a single power law is often assumed for the magnetic power spectra in the frequency range $10^{-4} - 10^{-1}$ Hz (Bruno & Carbone 2005; Bruno & Carbone 2013), although a few studies have found variation in the power law exponents in the inertial range of magnetic power spectra (Wicks et al. 2011; Sioulas et al. 2023b) as well as the scaling of higher order structure functions (Wu et al. 2022; Sorriso-Valvo et al. 2023). In our study, the co-existence of the two sub-regimes (with $-3/2$ and $-5/3$ spectral indices) within the turbulence spectra of FSW has been consistently observed at various heliospheric distances both in the inner as well as the outer heliosphere. The break scale between those two sub-ranges, $f_b$, appears to shift towards lower frequencies (approaching the correlation scale) with increasing heliospheric distance. This is consistent with the fact that a $-3/2$ scaling has been observed for solar wind close to the sun, whereas a steeper $-5/3$ power law is obtained at and beyond 1 au (Chen et al. 2020; Shi, C. et al. 2021; Sioulas et al. 2023a). Finally, in the Ulysses intervals, the ion-scale breaks are visible, separating the MHD range from the sub-ion range, where Hall effects and other kinetic effects start to affect the cascade (white background) (Banerjee & Galtier 2016; Halder et al. 2023). Such break is usually observed at frequencies $\sim 10^{-1}$ Hz, which is the upper cut-off for the MHD range. However, similar breaks do not turn up in the Helios intervals, due to the low cadence of the data used here.

To further investigate on the sub-inertial range spectral break, $f_b$, we study the kurtosis $K(\tau)$ for all of the eight FSW intervals. The scaling of $K(\tau)$ defined in Section 3 for Helios and Ulysses data are depicted in Fig. 4 top and bottom panels, respectively, for each $R$. To inspect on the general radial trend of intermittency we have drawn a consolidated plot for the Helios and Ulysses intervals (see Fig. 5). From this figure one can conclude that the value of $K$ at all scales increases with increasing $R$, thus implying higher intermittency with increasing heliospheric distance, in agreement with previous studies (Bruno et al. 2003; Sorriso-Valvo et al. 2023; Sioulas et al. 2023a). At each given distance $R$, $K$ is systematically found to decrease as one moves towards the larger scales. This is consistent with the notion that deviation from Gaussian statistics increases at smaller scales (Frisch 1995; Sorriso-Valvo et al. 1999). Upon reaching the typical correlation scales of the flow ($\tau \simeq 10^4$ s), corresponding to the $f^{-1}$ power law in energy spectrum (see Fig. 3), the kurtosis saturates to a constant value $K \simeq 1.67$, representing a quasi-Gaussian distribution (with a non-zero skewness) of the fluctuations of the magnetic field components (see appendix Section A). Within the inertial range, from the nature of $K(\tau)$ in Fig. 4, a clear signature of broken power law is observed. While two breaks are visible for Ulysses data (with 1 s resolution), the small-scale break at around $\tau \sim 10$ s is missing for the intervals using Helios magnetic field data with 6 s resolution. This break, corresponding to a frequency of $\sim 10^{-1}$ Hz, is associated

**Table 2.** Variation of the break scales observed in Kurtosis ($K$) scaling, $\tau_K$, and in magnetic power spectra, $f_b$, as a function of heliospheric distance $R$.

| $R$ (au) | 0.3 | 0.41 | 0.65 | 0.98 | 1.44 | 2.1 | 2.75 |
|---|---|---|---|---|---|---|---|
| $f_b$ (Hz) $(\times 10^{-3})$ | 14 | 8.2 | 8 | 6.9 | 3.8 | 0.7 | 0.7 |
| $\tau_K$ (s) | 84 | 140 | 214 | 374 | 499 | 799 | 1510 |

with the transition from the ordinary MHD range to the sub-ion kinetic or Hall MHD regime (Banerjee & Galtier 2016; Halder et al. 2023). The other break which occurs at a larger $\tau$ (solid vertical lines) is clearly visible for both Helios and Ulysses data. In particular this break scale ($\tau_K$) shifts towards larger $\tau$ as $R$ increases. Within the distance range of $0.3-2.75$ au, $\tau_K$ is found to increase from $\sim 100$ s to $\sim 1500$ s. It is to be emphasized here that except for certain cases, the appearance of the break $\tau_K$ is persistent in the component-wise $K$ scaling as well (see Figs. 10 and 11 in appendix Section B). A detailed list of the break scale $\tau_K$ as a function of $R$ is given in Table 2. As it is evident from Fig. 4 and 5, $\tau_K$ separates the steeper power law ($K \sim \tau^{-\kappa}$ with $\kappa \simeq 0.37$ averaged over the eight intervals) at smaller scales (dashed lines) from the less steeper one ($\kappa \simeq 0.11$ on average) at large scales (dotted lines), but with an exception. Note that for the Ulysses interval at $R = 3.16$ au, $K(\tau)$ reaches the Gaussian regime without going through the large $\tau$ break, suggesting that the turbulence has fully developed that transforms the shallower scaling range at large scale into the steeper power law at smaller scales. We will elucidate this point in the following.

As mentioned in the introduction, similar broken power law behaviour for $K(\tau)$ in FSW has already been observed by Sorriso-Valvo et al. (2023). However, those authors suggested that $\tau_K$ might correspond to the break between low-frequency $f^{-1}$ regime to Kolmogorov $f^{-5/3}$ regime in the magnetic power spectra. This was inspired by the fact that $f^{-1}$ regime is exclusively found in FSW intervals and the $f^{-1}$ break also shows nearly similar behaviour to $1/\tau_K$ as $R$ changes (Davis et al. 2023). Instead, for all the intervals where the break is observed, it is systematically found in our study that $1/\tau_K$ occurs at a higher frequency (roughly by a factor $\sim 10$) than the $f^{-1}$ break scale (see Fig. 3). The inverse of $\tau_K$ is typically corresponding to $f_b$, although with some consistent small discrepancy that could be due to the different frequency response of Fourier transform and scale-dependent increments (see Fig. 4 where both $\tau_K$, solid lines, and $1/f_b$, dashed lines, are drawn). The two scaling ranges in the kurtosis therefore approximately correspond to the two inertial sub-ranges observed in the spectrum. Since $PSD$ and kurtosis are related quantities, the observation of a double power law in both supports the robustness of the break, and therefore indicates the emergence of a new characteristic scale in the inertial range that marks the transition from $f^{-3/2}$ to $f^{-5/3}$ regime.

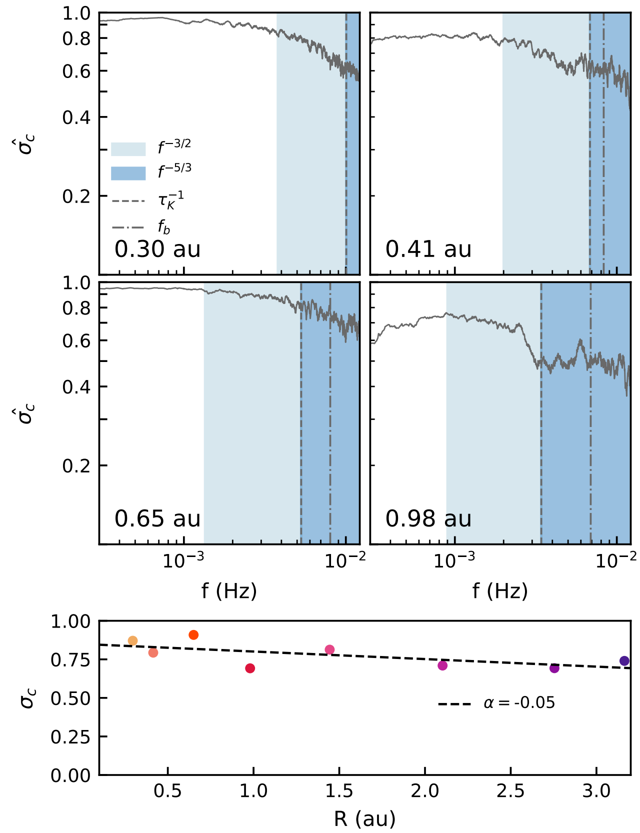


**Figure 6.** Top: Normalized cross-helicity spectrum $\hat{\sigma_c}$ (smoothed using a running mean window) of the four Helios FSW intervals in the inner heliosphere. The light and deep blue shaded regions depict the $-3/2$ and $-5/3$ regimes respectively. The spectral break frequency $f_b$ and the frequency associated with the kurtosis break, $\tau_K^{-1}$, are indicated by dot-dashed and dashed lines respectively. Bottom: Cross-helicity $\sigma_c$ of all the FSW intervals as a function of the heliospheric distance $R$.

Summarizing, from the existence of the two turbulent inertial sub-regimes it is clear that as we move from the larger towards the smaller scales the nature of turbulence also varies. This variation becomes more apparent when we examine the cross-helicity spectrum for the FSW intervals within the inner heliosphere (Fig. 6 top). The same could not be computed for the FSW beyond 1 au due to the limitation in terms of low plasma data resolution, as mentioned in Section 2. Nevertheless, for all the FSW intervals in the inner heliosphere we see that the $\hat{\sigma}_c$ power decreases as we move from larger

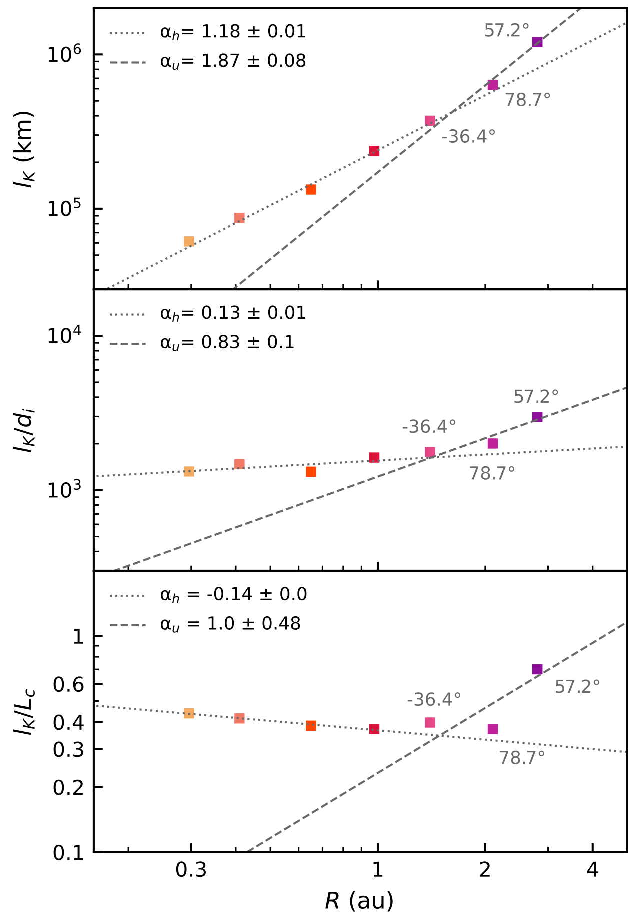


**Figure 7.** FSW during solar minima. Top: Kurtosis scaling break $l_K (= V_{sw}\tau_K)$ versus the heliospheric distance $R$. The same break scale $l_K$ normalized by the ion-inertial length scale $d_i$, $l_K/d_i$ (middle) and $l_K$ normalized by the correlation length $L_c$ (bottom) as a function of $R$. The different colors reproduce the colors in Fig. 3, and in the Ulysses intervals the latitude is indicated. Two power laws were identified in the inner and outer heliosphere, respectively. The fitted power laws and the corresponding parameters are indicated.

to smaller scales (see Fig. 6). Thus, with the forward progression of the turbulent cascade, the imbalance between the inward and outward Alfvén modes propagating along the mean magnetic field decreases to a more balanced state. While recent studies have shown the transition from a weak to a strong turbulence regime on moving towards smaller scales (Zhao et al. 2024), a transition from imbalanced ($|z^{+2}| \gg |z^{-2}|$, or vice-versa) to a balanced ($|z^{+2}| \sim |z^{-2}|$) turbulent state could as well be associated with the steepening of the spectra from the low frequency $f^{-3/2}$ regime to the higher frequency $f^{-5/3}$ regime. A similar gradual change from an imbalanced towards a relatively balanced state is also evident with increasing heliospheric distance $R$. Even though $\sigma_c$ $(= \frac{\langle \delta\mathbf{v}\cdot\delta\mathbf{b}\rangle}{\langle|\delta\mathbf{v}|^2+|\delta\mathbf{b}|^2\rangle}$, where $\langle\cdot\rangle$ is done over the interval) shows sufficiently higher values being associated with FSW, it declines slowly as understood from the straight line fit having a slope $\alpha = -0.05$ (see Fig. 6 bottom). This is again consistent with the absence of the $f^{-3/2}$ regime at $R = 3.16$ au and recent observations of change in the inertial range spectral index from $-3/2$ to $-5/3$ with increasing $R$ (Chen et al. 2020; Shi, C. et al. 2021; Sioulas et al. 2023a).

We further determine the evolutionary nature of the break scale, $\tau_K$, with $R$ and have investigated its relationship with the typical ion and correlation scales. In Fig. 7 (top), we show the radial evolution of $\tau_K$, appearing in the scaling of $K$, converted from time scale to length scale ($l_K$) via Taylor's hypothesis as mentioned in Section 3. Clearly, $l_K$ shift towards larger scales with $R$, as evident from Fig. 5 and Table 2 as well. We see that a strong power-law relation exists between $R$ and $l_K$, with $l_K$ evolving as $l_K \propto R^{1.18}$ for $R < 1$ au and $l_K \propto R^{1.87}$ for $R > 1$ au. The central panel in Fig. 7 shows how the break scale behaves with $R$ when normalized to the ion-inertial length scale, $d_i = c/\omega_{pi}$ (where $\omega_{pi} = \sqrt{ne^2/\epsilon_0 m}$ is the plasma frequency). The ion-inertial scale has been found to vary between $\sim 45$ to $\sim 500$ km for $R$ ranging from $R \simeq 0.3$—$3.2$ au. After normalization, we find that the evolutionary nature is nearly lost for FSW intervals in the inner heliosphere near the ecliptic plane, with a residual weak $R^{0.13}$ dependence, and $l_K$ is $\sim 10^3$ times $d_i$. A similar pattern was observed (but not shown) after normalization with the ion gyro-radius $\rho_i = v_{th}^{\perp}/\Omega_i$, in the inner heliosphere (the $\rho_i$ in the outer heliosphere could not be computed again due to data limitations). Note that the typical ion scales have an approximately linear radial increase up to 5 au (e.g., see Bruno & Trenchi 2014) which might explain the constant radial trend of the normalized break scale. However, beyond 1 au, it is to be noted that even after normalization, the evolutionary nature of $l_K$ still persists, so that only the radial trend of the break decouples from that of the ion scales. The residual power law could be associated with the variation in heliospheric latitude (and to the associated variation of the angle between the large-scale magnetic field $B$ and the bulk speed $V_{sw}$) at which the FSW streams were sampled, indicated in the labels in Fig. 7. Understanding this variation of $l_K$ with latitude and $V_{sw}$-$B$ angle would be interesting for a future study but is currently beyond the scope of this paper. In order to compare the break scale $l_K$ and the correlation scale $L_c$, we have drawn $l_K$ normalized to $L_c$ as a function of $R$ (see Fig. 7 bottom). Here $L_c$ is the Taylor-shifted $\tau_c$, which is the time lag at which the trace of the correlation matrix of $\mathbf{B}$ decreases exponentially. It is evident from the

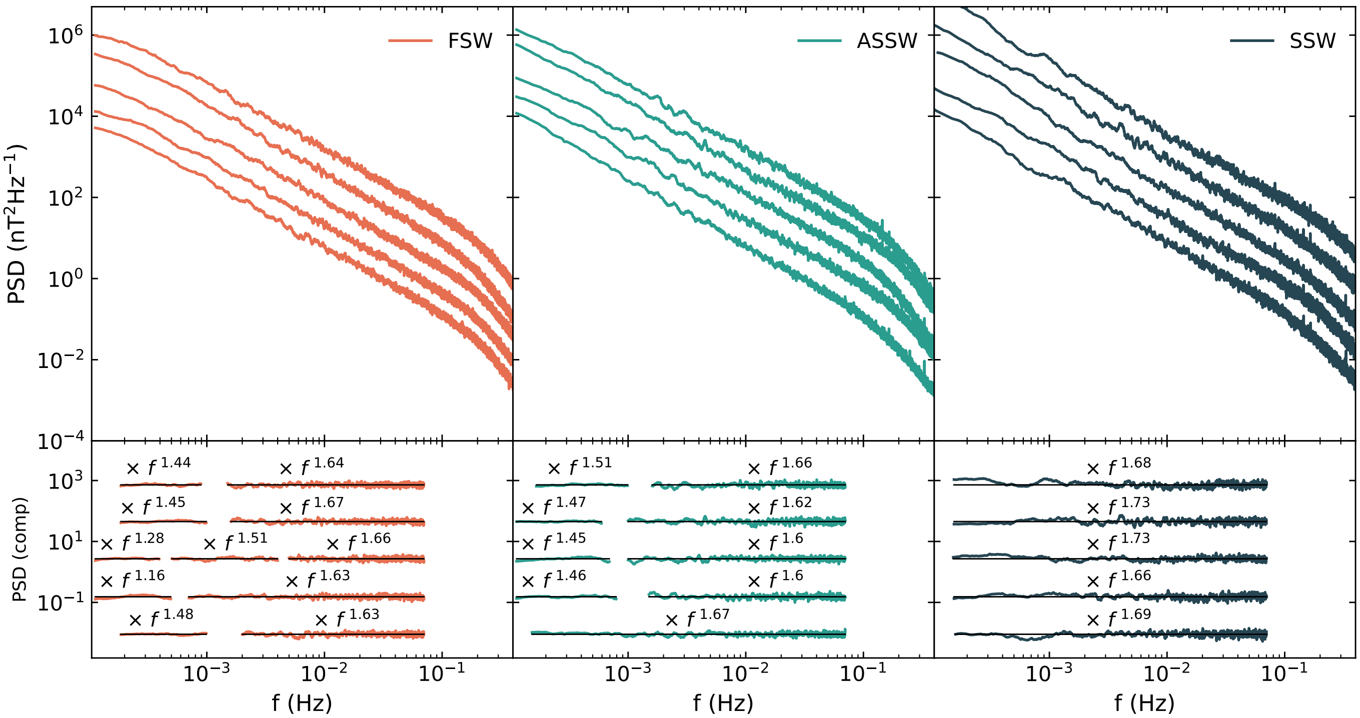


**Figure 8.** Magnetic field power spectral trace (smoothed using a running mean window) of the FSW, ASSW & SSW intervals tabulated in Table-1 during solar maximum (the PSD's are artificially shifted for representation). The SSW exhibits a broad inertial range while different power law breaks are present in the case of ASSW & FSW. In each range, the compensated spectra is shown along with the corresponding spectral exponent.

plot that, for $R < 1$, a small power-law exponent is observed, $l_K/L_c \sim R^{-0.14}$, so that the normalization to the correlation scale removes the radial dependence, similar to what we observe when normalized to the ion scale. Moreover, in this case, $l_K$ is $\sim 0.4$ times $L_c$ and certainly does not correspond to scales within the $f^{-1}$ power law regime in the spectrum, contrary to what has been suggested previously (Sorriso-Valvo et al. 2023). For $R > 1$, $l_K$ approaches $L_c$, thereby explaining the absence of the $f^{-3/2}$ regime in the $R = 3.16$ au interval and supporting recent observations of spectral steepening of the inertial range with increasing $R$ (Chen et al. 2020; Shi, C. et al. 2021; Sioulas et al. 2023a). Note that, in the inner heliosphere, break scales normalized to both the characteristic ion scale and the correlation scale follow weak radial dependence of $R^{0.13}$ and $R^{-0.14}$, respectively.

### 4.2. *Observations during Solar Maximum*

We now perform a similar spectral and intermittency analysis using the set of intervals recorded during the solar maximum (see Table 1). While the previous section was confined to only analyzing FSW, in this section we take into consideration the three main solar wind types, namely FSW, SSW and the ASSW. Previous studies on spectra and intermittency mostly focused on FSW and SSW (Bruno et al. 2003; Di Mare et al. 2019; Carbone et al. 2021; Sorriso-Valvo et al. 2021). More recently, the spectral properties of ASSW, which exclusively permeates the heliosphere during periods of high solar activity, were also examined (D'Amicis et al. 2021, 2022). However, such studies did not include intermittency. Moreover, a comparative analysis between FSW, SSW and ASSW at solar maxima has not yet been conducted. Thus, in this section, we examine the intermittency properties of ASSW (Marsch et al. 1981; D'Amicis et al. 2011; D'Amicis & Bruno 2015) in comparison with the other two types of wind using Ulysses data, during the ascending phase of solar cycle 23 (year 2001), at $R \simeq 1.5$ au.

In Fig. 8, the smoothed magnetic power spectra have been shown for all of the intervals tabulated in Table 1. In contrast to the solar minima where systematically two regimes with $f^{-3/2}$ and $f^{-5/3}$ were found, during solar maximum we find FSW intervals both with and without the $f^{-3/2}$ regime. This could be due to the fact that the break between the $f^{-3/2}$ and $f^{-5/3}$ regime has evolved to larger scales beyond the correlation scale of turbulence which was measured to be $\sim 1250$ s ($8 \times 10^{-4}$ Hz) for these intervals. A similar observation was made in the previous section for the interval at $R = 3.16$ au. For ASSW, the $f^{-3/2}$ regime is also evident

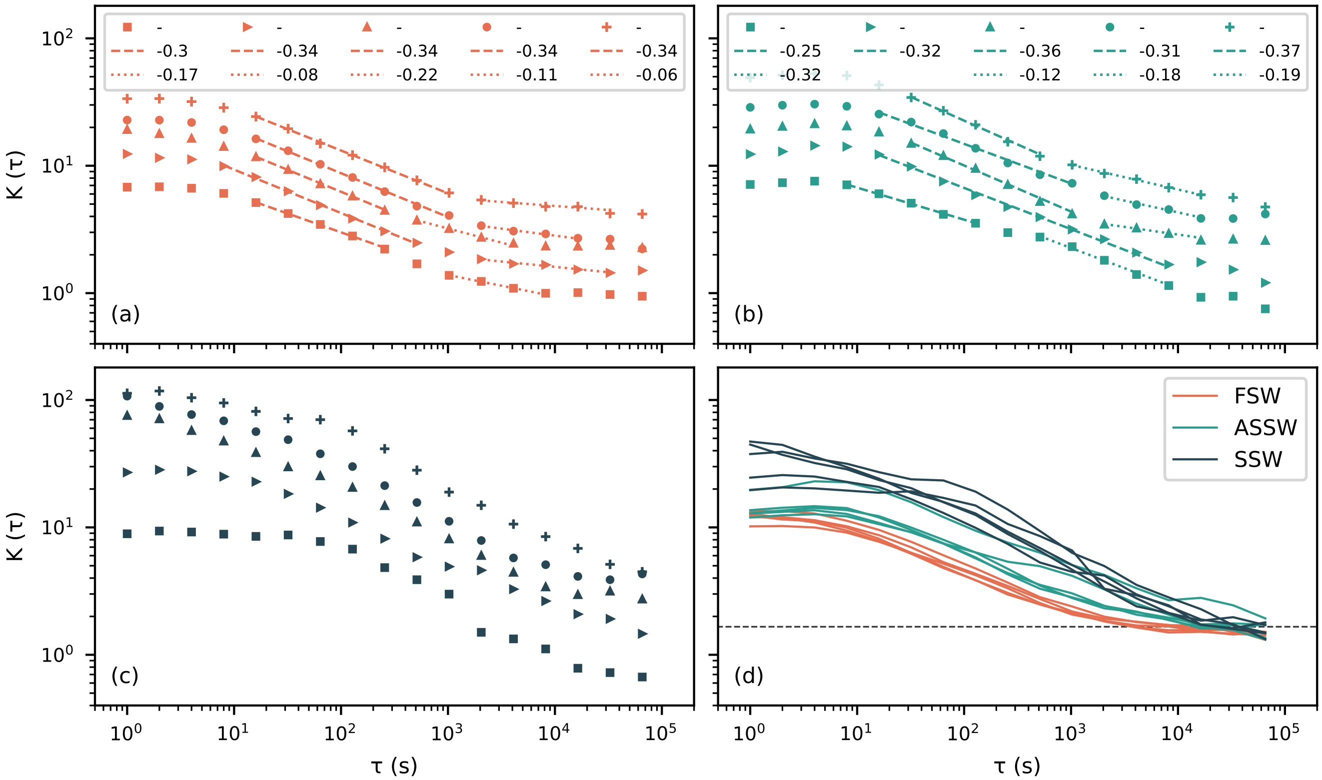


**Figure 9.** Kurtosis ($K$) of the magnetic field fluctuations as a function of time scale ($\tau$) for several intervals of (a) FSW (orange), (b) ASSW (green) and (c) SSW (deep blue), during solar maximum. In panels (a), (b) and (c), the kurtosis for each interval have been artificially shifted for better representation while panel (d) shows a consolidated plot of all the intervals (with no artificial shifting) of the three types of solar wind.

in the spectra for most of the intervals. However, the $f^{-1}$ regime is not apparent as the correlation scale in this case is $\sim 5000$ s ($2 \times 10^{-4}$ Hz). On the other hand, the spectra of the SSW intervals exhibit a broad $f^{-5/3}$ regime extending to much lower frequencies with the $f^{-1}$ and $f^{-3/2}$ regimes being absent.

The variation of $K$ (defined in Section 3) as a function of $\tau$ is shown in Fig. 9 for all the aforementioned intervals. Similar to what has been observed during solar minima, $K$ is found to be scale dependent, decreasing with the time scale $\tau$ and approaching the Gaussian value $K \simeq 1.67$ at $\tau >\sim 10^4$ s (See appendix A). This is again a clear indication of the non-universal nature of the distribution function of the magnetic field increments. From Fig. 9 (a), (b) & (c), it is evident that a steeper power law followed by a shallower one is commonly observed for FSW and ASSW, while for SSW the shape varies quite a lot and it is hard to determine distinct regimes. The two power law regimes existing for FSW and ASSW are fairly consistent with the existence of two distinct regimes in the spectra of these two types of wind (for more details see Section 4.1). Moreover, for many intervals, the break in the kurtosis corresponds well to that in the power spectra between the $f^{-5/3}$ & the $f^{-3/2}$ regime in both FSW and ASSW implying a close relation between them. For SSW, where distinct regimes in kurtosis are not observed, the spectra is found to exhibit a broad $f^{-5/3}$ regime.

The consolidated plot shown in Fig. 9 (d) allows to perform a comparative study of intermittency among those three types of solar wind. As evident from the plots, turbulence in ASSW is moderately intermittent, characterized by a value of $K$ which is intermediate between that of the SSW with the strongest intermittency and that of the FSW having the weakest intermittency. Our observations are in agreement with the fact that, in the outer heliosphere, the SSW is in a state of more developed turbulence. This can also be inferred from the broad inertial range in the magnetic power spectra exhibited by SSW extending to much lower frequencies compared to FSW and ASSW.

Interestingly, a recent study conducted by D'Amicis et al. (2018) observes a $f^{-1}$ break in the spectra of ASSW at 1 au. It clearly shows how the turbulence develops in ASSW by the broadening of the inertial range as it evolves with $R$. While studies by D'Amicis & Bruno (2015); D'Amicis et al. (2018); D'Amicis et al. (2021) explain the high Alfvénicity of ASSW as due to its generation from coronal hole boundaries based on its composition and micro-physics, our findings on ASSW with an intermediate state of turbulence hints that the low speed of ASSW may be due to the intermixing of FSW and SSW inside the heliosphere.

## 5. SUMMARY AND CONCLUSION

In this paper, we report the existence of two distinct sub-regimes for the inertial range in the magnetic power spectrum of solar wind turbulence within and beyond 1 au. Although a single inertial range spectral power law has been traditionally observed (Bruno & Carbone 2013), a few studies have also identified variations in the spectral indices of the magnetic power spectrum (Wicks et al. 2011; Sioulas et al. 2023b) and in the scaling exponents of higher-order structure functions (Wu et al. 2022, 2023). Additionally, Sorriso-Valvo et al. (2023) observed a break ($\tau_K$) in the scaling of kurtosis ($K$) within FSW intervals, suggesting a possible connection between this break and the $f^{-1}$ break due to their similar behavior with $R$ as discussed by Davis et al. (2023). However, our findings show that $\tau_K$ in the kurtosis scaling closely coincides with the break ($f_b$) observed in magnetic spectra separating the two sub-regimes characterized by $f^{-3/2}$ and $f^{-5/3}$ spectral power laws in both the inner as well as the outer heliosphere (see Fig. 4). The appearance of a double power-law in both the magnetic power spectrum and kurtosis (or normalized fourth-order moments) supports the robustness of this break, indicating the existence of a previously unidentified characteristic scale within the inertial range. Whereas the most probable explanation for the $f^{-5/3}$ regime can be obtained by the isotropic Kolmogorov phenomenology or anisotropic mhd turbulence with a weak **v-b** alignment in non-Alfvénic solar wind, the $f^{-3/2}$ regime could be reasonably associated with the anisotropic spectra along the strong **v-b** alignment (Kolmogorov 1941; Goldreich & Sridhar 1995; Boldyrev 2006). Note that, we consciously eliminate the possibility of a $-3/2$ spectra by Iroshnikov-Kraichnan phenomenology which is valid only for balanced MHD and cannot explain the emergence of $-3/2$ spectra when there is a strong **v-b** correlation.

A recent study by Zhao et al. (2024) provided evidence of a transition from a weak to a strong turbulence regime as one moves from larger to smaller scales. In our study, an inspection of the cross-helicity co-spectra revealed that the turbulence in FSW shifts from a highly imbalanced state ($|z^{+2}| \gg |z^{-2}|$, or vice-versa) at larger scales to a relatively balanced one ($|z^{+2}| \sim |z^{-2}|$) on moving towards the smaller scales (see Fig. 6). These observations may explain the broken power-law behavior of the spectrum and the kurtosis indicating a transition in the nature of turbulence as the cascade progresses towards the smaller scales.

We have further investigated the dependence of the sub-inertial regime break ($\tau_K$) on the heliospheric distance ($R$) in comparison with the ion and correlation scales. Our findings indicate a power-law behavior for $l_K$ (Taylor transformed $\tau_K$, Taylor 1938) with $R$, which upon normalization with the typical ion scales (e.g. the ion-inertial scale $d_i$ and the ion gyro-radius $\rho_i$) and the correlation scale ($L_c$) practically disappears in the inner heliosphere (see Fig. 7). Therefore, both the correlation scale and the characteristic ion scale appear to control the location of the break. Interestingly, though, $l_K$ appears to approach the correlation scale shifting towards larger scales as $R$ increases, resulting in the absence of the $f^{-3/2}$ regime at 3.16 au. This observation could explain the transition of the inertial range magnetic spectral slope from $-3/2$ near the Sun to $-5/3$ farther away (Chen et al. 2020; Shi, C. et al. 2021; Sioulas et al. 2023a). Note that a residual power-law radial dependence of the break scale still persists in the outer heliosphere, possibly due to variations in the latitude at which the FSW streams were sampled. This residual behaviour of the normalized $l_K$ must be studied in depth in a future study as functions of the latitude and also the large-scale magnetic field angle, which determines the degree of anisotropy in the measured turbulence.

Our analysis during high solar activity enables us to characterize the state of turbulence in the Alfvénic slow solar wind, as compared to traditional fast and slow winds. ASSW, which is found in abundance near the ecliptic plane, is in an intermediate state of turbulence between typical fast and slow streams. This also gives us insights on the position of the break separating the integral ($f^{-1}$) and inertial ranges (Matthaeus & Goldstein 1986; Chandran 2018) in the case of ASSW. While D'Amicis et al. (2018) found the $f^{-1}$ break to be occurring at the same frequency for FSW as well as ASSW at 1 au, in our study it occurs at a much lower frequency for the ASSW compared to the FSW at distances greater than 1.5 au (see Fig. 8), thus suggesting a plausible explanation for the 'slowness' of the ASSW due to strong intermixing between the FSW and the SSW during the high solar activity.

ACKNOWLEDGMENTS

S.M. was supported by Students-Undergraduate Research Graduate Excellence (SURGE) summer internship program at Indian Institute of Technology Kanpur. S.B. acknowledges the financial support from the grant by Space Technology Cell-ISRO (STC/PHY/2023664O). L.S.-V. received support by the Swedish Research Council (VR) Research Grant N. 2022-03352 and by the International Space Science Institute (ISSI) in Bern, through ISSI International Team project #23-591 (Evolution of Turbulence in the Expanding Solar Wind).

## DATA AVAILABILITY

For our study, we have used publicly available data from NASA CDAWeb (https://cdaweb.gsfc.nasa.gov) and AMDA science analysis system (https://amda.irap.omp.eu).

# APPENDIX

## A. ESTIMATION OF KURTOSIS OF MAGNETIC FIELD FLUCTUATIONS FOLLOWING A GAUSSIAN DISTRIBUTION

Following the definition of the $n^{th}$ order structure function ($S_n$) given by eqn. (1), the expression of $S_4$ and $S_2$ takes the form:

$$S_4 = ((\Delta b_r)^2 + (\Delta b_t)^2 + (\Delta b_n)^2)^2, \tag{A1}$$

and

$$S_2 = ((\Delta b_r)^2 + (\Delta b_t)^2 + (\Delta b_n)^2), \tag{A2}$$

respectively. Now considering that the fluctuations follow a zero mean gaussian distribution $f(\Delta b_i)$ having a standard deviation $\sigma$ such that

$$f(\Delta b_i) = \frac{1}{\sqrt{2\pi\sigma^2}} exp\left[\frac{(\Delta b_i)^2}{2\sigma^2}\right], \tag{A3}$$

we have

$$S_4 = \int\int\int ((\Delta b_r)^2 + (\Delta b_t)^2 + (\Delta b_n)^2)^2 f(\Delta b_r) f(\Delta b_t) f(\Delta b_n)\, d(\Delta b_r)\, d(\Delta b_t)\, d(\Delta b_n), \tag{A4}$$

and

$$S_2 = \int\int\int ((\Delta b_r)^2 + (\Delta b_t)^2 + (\Delta b_n)^2) f(\Delta b_r) f(\Delta b_t) f(\Delta b_n)\, d(\Delta b_r)\, d(\Delta b_t)\, d(\Delta b_n), \tag{A5}$$

which seem a bit rigorous but can be solved easily to obtain $S_4 = 15\sigma^4$ and $S_2 = 3\sigma^2$. Thus, the kurtosis defined by eqn. (2) takes the value $K = 5/3 \simeq 1.67$.

## B. COMPONENT-WISE KURTOSIS OF THE MAGNETIC FIELD FLUCTUATIONS IN FSW INTERVALS DURING SOLAR MINIMUM

In this appendix we show the kurtosis $K$ for each individual RTN magnetic field component, using four example intervals from both Helios and Ulysses database, at eighth different distances from the Sun. Different colors refer to the different intervals. Whenever present, a power law is shown as colored dashed line, and the corresponding scaling exponents are indicated in each panel. Two power laws can be identified in all of the Helios and most of the Ulysses intervals, with the exception of the radial component at 2.75 au and of all components at 3.16 au. The timescale $\tau_K$ of the break between the two power laws is indicated by a solid vertical grey line, while the dashed grey vertical lines indicate the location of the spectral break, $1/f_b$.

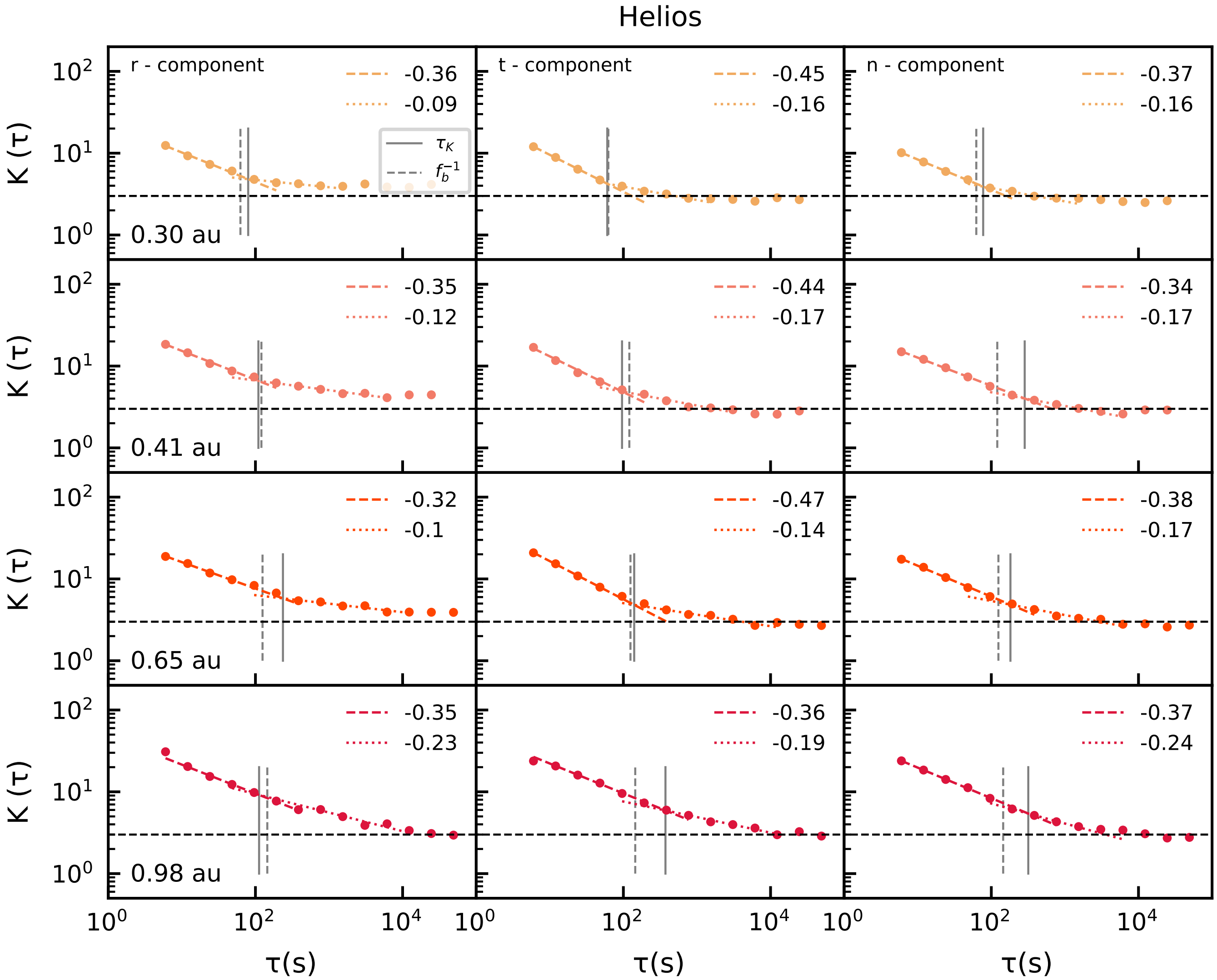


**Figure 10.** Component-wise kurtosis $K(\tau)$ of magnetic field fluctuations for several intervals of FSW during periods of solar minima for Helios data (year 1976) in the inner heliosphere from a sustained coronal hole. The three columns represent the r, t and n components of $K$. Power-law fits and the corresponding scaling exponents are indicated. Vertical lines indicate the observed break, $\tau_K$ (solid), and the timescale corresponding to the spectral break, $1/f_b$ (dashed).

## REFERENCES


Alberti, T., Laurenza, M., Consolini, G., et al. 2020, The Astrophysical Journal, 902, 84, doi: 10.3847/1538-4357/abb3d2

Alexandrova, O., Saur, J., Lacombe, C., et al. 2009, Phys. Rev. Lett., 103, 165003, doi: 10.1103/PhysRevLett.103.165003

Anselmet, F., Gagne, Y., Hopfinger, E. J., & Antonia, R. A. 1984, Journal of Fluid Mechanics, 140, 63–89, doi: 10.1017/S0022112084000513

Bale, S. D., Horbury, T. S., Velli, M., et al. 2021, ApJ, 923, 174, doi: 10.3847/1538-4357/ac2d8c

Banerjee, S. 2014, PhD thesis. http://www.theses.fr/2014PA112206

Banerjee, S., & Andrés, N. 2020, Phys. Rev. E, 101, 043212, doi: 10.1103/PhysRevE.101.043212

Banerjee, S., & Galtier, S. 2013, Phys. Rev. E, 87, 013019, doi: 10.1103/PhysRevE.87.013019

—. 2016, Journal of Physics A: Mathematical and Theoretical, 50, 015501, doi: 10.1088/1751-8113/50/1/015501

Banerjee, S., Hadid, L. Z., Sahraoui, F., & Galtier, S. 2016, The Astrophysical Journal Letters, 829, L27, doi: 10.3847/2041-8205/829/2/L27

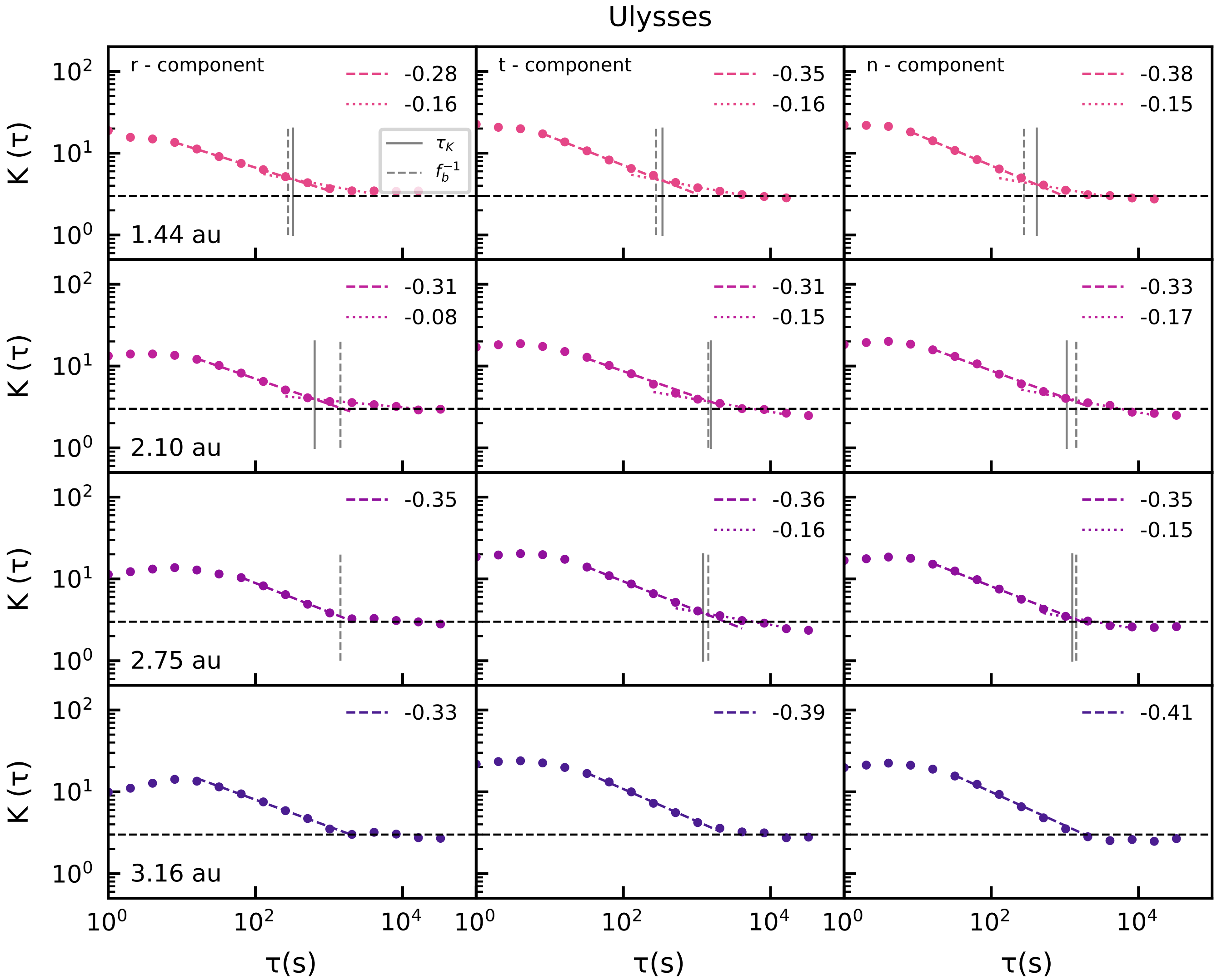


**Figure 11.** Component-wise kurtosis $K(\tau)$ of magnetic field fluctuations for several intervals of FSW during periods of solar minima for Ulysses data (years 1995-1996) in the outer heliosphere at varying distances and latitudes. The three columns represent the r, t and n components of $K$. Power-law fits and the corresponding scaling exponents are indicated. Vertical lines indicate the observed break, $\tau_K$ (solid), and the timescale corresponding to the spectral break, $1/f_b$ (dashed).

Bavassano, B., Dobrowolny, M., Fanfoni, G., Mariani, F., & Ness, N. F. 1982a, Solar Physics, 78, 373, doi: 10.1007/bf00151617

Bavassano, B., Dobrowolny, M., Mariani, F., & Ness, N. F. 1982b, Journal of Geophysical Research: Space Physics, 87, 3617, doi: https://doi.org/10.1029/JA087iA05p03617

Bavassano, B., Pietropaolo, E., & Bruno, R. 1998, J. Geophys. Res., 103, 6521, doi: 10.1029/97JA03029

Belcher, J. W. 1971, ApJ, 168, 509, doi: 10.1086/151105

Belcher, J. W., & Davis Jr., L. 1971, Journal of Geophysical Research (1896-1977), 76, 3534, doi: https://doi.org/10.1029/JA076i016p03534

Biskamp, D. 2003, Magnetohydrodynamic Turbulence (Cambridge University Press), doi: 10.1017/CBO9780511535222

Boldyrev, S. 2006, Phys. Rev. Lett., 96, 115002, doi: 10.1103/PhysRevLett.96.115002

Bruno, R., & Carbone, V. 2005, Living Reviews in Solar Physics, 10, 1. https://api.semanticscholar.org/CorpusID:121902748

Bruno, R., & Carbone, V. 2013, *Liv. Rev. in Solar Phys.*, 10, 2, doi: https://doi.org/10.12942/lrsp-2013-2

Bruno, R., Carbone, V., Sorriso-Valvo, L., & Bavassano, B. 2003, Journal of Geophysical Research (Space Physics), 108, 1130, doi: 10.1029/2002JA009615

Bruno, R., & Trenchi, L. 2014, The Astrophysical Journal Letters, 787, L24, doi: 10.1088/2041-8205/787/2/L24

Bruno, R., Telloni, D., Sorriso-Valvo, L., et al. 2019, A&A, 627, A96, doi: 10.1051/0004-6361/201935841

Carbone, F., Sorriso-Valvo, L., Khotyaintsev, Yu. V., et al. 2021, A&A, 656, A16, doi: 10.1051/0004-6361/202140931

Chandran, B. D. G. 2018, Journal of Plasma Physics, 84, 905840106, doi: 10.1017/S0022377818000016

Chandran, B. D. G., Schekochihin, A. A., & Mallet, A. 2015, The Astrophysical Journal, 807, 39, doi: 10.1088/0004-637X/807/1/39

Chen, C. H. K., Bale, S. D., Bonnell, J. W., et al. 2020, The Astrophysical Journal Supplement Series, 246, 53, doi: 10.3847/1538-4365/ab60a3

Cranmer, S. R., Matthaeus, W. H., Breech, B. A., & Kasper, J. C. 2009, The Astrophysical Journal, 702, 1604, doi: 10.1088/0004-637X/702/2/1604

D'Amicis, R., & Bruno, R. 2015, The Astrophysical Journal, 805, 84, doi: 10.1088/0004-637X/805/1/84

D'Amicis, R., Bruno, R., & Bavassano, B. 2011, Journal of Atmospheric and Solar-Terrestrial Physics, 73, 653, doi: https://doi.org/10.1016/j.jastp.2011.01.012

D'Amicis, R., Matteini, L., & Bruno, R. 2018, Monthly Notices of the Royal Astronomical Society, 483, 4665, doi: 10.1093/mnras/sty3329

D'Amicis, R., Perrone, D., Velli, M., et al. 2022, Universe, 8, 352, doi: 10.3390/universe8070352

D'Amicis, R., Bruno, R., Panasenco, O., et al. 2021, A&A, 656, A21, doi: 10.1051/0004-6361/202140938

Davis, N., Chandran, B. D. G., Bowen, T. A., et al. 2023, The Astrophysical Journal, 950, 154, doi: 10.3847/1538-4357/acd177

Di Mare, F., Sorriso-Valvo, L., Retinò, A., Malara, F., & Hasegawa, H. 2019, Atmosphere, 10, doi: 10.3390/atmos10090561

Frisch, U. 1995, Turbulence: The Legacy of AN Kolmogorov (Cambridge University Press)

Goldreich, P., & Sridhar, S. 1995, ApJ, 438, 763, doi: 10.1086/175121

Goldreich, P., & Sridhar, S. 1997, The Astrophysical Journal, 485, 680, doi: 10.1086/304442

Halder, A., Banerjee, S., Chatterjee, A. G., & Sharma, M. K. 2023, Phys. Rev. Fluids, 8, 053701, doi: 10.1103/PhysRevFluids.8.053701

Hellinger, P., Matteini, L., Štverák, Š., Trávníček, P. M., & Marsch, E. 2011, Journal of Geophysical Research (Space Physics), 116, A09105, doi: 10.1029/2011JA016674

Hernández, C. S., Sorriso-Valvo, L., Bandyopadhyay, R., et al. 2021, The Astrophysical Journal Letters, 922, L11, doi: 10.3847/2041-8213/ac36d1

Iroshnikov, P. S. 1963, AZh, 40, 742

Kolmogorov, A. 1941, Akademiia Nauk SSSR Doklady, 30, 301

Kolmogorov, A. N. 1962, Journal of Fluid Mechanics, 13, 82–85, doi: 10.1017/S0022112062000518

Kraichnan, R. H. 1965, The Physics of Fluids, 8, 1385, doi: 10.1063/1.1761412

Marino, R., & Sorriso-Valvo, L. 2023, Physics Reports, 1006, 1, doi: https://doi.org/10.1016/j.physrep.2022.12.001

Marsch, E., Mühlhäuser, K.-H., Rosenbauer, H., Schwenn, R., & Denskat, K. U. 1981, Journal of Geophysical Research: Space Physics, 86, 9199, doi: https://doi.org/10.1029/JA086iA11p09199

Marsch, E., Mühlhäuser, K.-H., Schwenn, R., et al. 1982, Journal of Geophysical Research: Space Physics, 87, 52, doi: https://doi.org/10.1029/JA087iA01p00052

Matthaeus, W. H., & Goldstein, M. L. 1986, Phys. Rev. Lett., 57, 495, doi: 10.1103/PhysRevLett.57.495

Perrone, D., Stansby, D., Horbury, T. S., & Matteini, L. 2018, Monthly Notices of the Royal Astronomical Society, 483, 3730, doi: 10.1093/mnras/sty3348

Phillips, J. L., Bame, S. J., Feldman, W. C., et al. 1995, Science, 268, 1030, doi: 10.1126/science.268.5213.1030

Podesta, J. J., & Borovsky, J. E. 2010, Physics of Plasmas, 17, 112905, doi: 10.1063/1.3505092

Podesta, J. J., Roberts, D. A., & Goldstein, M. L. 2006, Journal of Geophysical Research: Space Physics, 111, doi: https://doi.org/10.1029/2006JA011834

Pope, S. 2000, Turbulent Flows (Cambridge University Press). https://books.google.com/books?id=HZsTw9SMx-0C

Roberts, D. A. 2010, Journal of Geophysical Research: Space Physics, 115, doi: https://doi.org/10.1029/2009JA015120

Roberts, D. A., Goldstein, M. L., Matthaeus, W. H., & Ghosh, S. 1992, J. Geophys. Res., 97, 17115, doi: 10.1029/92JA01144

Sakshee, S., Bandyopadhyay, R., & Banerjee, S. 2022, Monthly Notices of the Royal Astronomical Society, 514, 1282, doi: 10.1093/mnras/stac1449

Shi, C., Velli, M., Panasenco, O., et al. 2021, A&A, 650, A21, doi: 10.1051/0004-6361/202039818

Sioulas, N., Huang, Z., Velli, M., et al. 2022, The Astrophysical Journal, 934, 143, doi: 10.3847/1538-4357/ac7aa2

Sioulas, N., Huang, Z., Shi, C., et al. 2023a, The Astrophysical Journal Letters, 943, L8, doi: 10.3847/2041-8213/acaeff

Sioulas, N., Velli, M., Huang, Z., et al. 2023b, The Astrophysical Journal, 951, 141, doi: 10.3847/1538-4357/acc658

Smith, E. J., Tsurutani, B. T., & Rosenberg, R. L. 1978, Journal of Geophysical Research: Space Physics, 83, 717, doi: https://doi.org/10.1029/JA083iA02p00717

Sorriso-Valvo, L., Carbone, V., Veltri, P., Consolini, G., & Bruno, R. 1999, Geophys. Res. Lett., 26, 1801, doi: 10.1029/1999GL900270

Sorriso-Valvo, L., Marino, R., Foldes, R., et al. 2023, A&A, 672, A13, doi: 10.1051/0004-6361/202244889

Sorriso-Valvo, L., Yordanova, E., Dimmock, A. P., & Telloni, D. 2021, The Astrophysical Journal Letters, 919, L30, doi: 10.3847/2041-8213/ac26c5

Sorriso-Valvo, L., Marino, R., Carbone, V., et al. 2007, Phys. Rev. Lett., 99, 115001, doi: 10.1103/PhysRevLett.99.115001

Taylor, G. I. 1938, Proceedings of the Royal Society of London. Series A - Mathematical and Physical Sciences, 164, 476, doi: 10.1098/rspa.1938.0032

Telloni, D. 2022, Frontiers in Astronomy and Space Sciences, 9, doi: 10.3389/fspas.2022.917393

Tu, C.-Y., & Marsch, E. 1995, Space Science Reviews, 73, 1

Wicks, R. T., Horbury, T. S., Chen, C. H. K., & Schekochihin, A. A. 2011, Phys. Rev. Lett., 106, 045001, doi: 10.1103/PhysRevLett.106.045001

Wu, H., He, J., Yang, L., et al. 2022, On the scaling and anisotropy of two subranges in the inertial range of solar wind turbulence. https://arxiv.org/abs/2209.12409

Wu, H., Huang, S., Wang, X., et al. 2023, The Astrophysical Journal Letters, 947, L22, doi: 10.3847/2041-8213/acca20

Zhao, S., Yan, H., Liu, T. Z., Yuen, K. H., & Wang, H. 2024, Nature Astronomy, 8, 725, doi: 10.1038/s41550-024-02249-0